J. Astron. Space Sci. 16(2), 149 – 158 (1999)

OBSERVATIONS OF TERRESTRIAL NIGHTGLOW (MEINEL BANDS) AT KING SEJONG STATION, ANTARCTICA

Young-In Won, Young-Min Cho, Bang Yong Lee[1], Jhoon Kim[2], Jong Kyun Chung, Yong Ha Kim[3]
[1]Polar Research Center, Korea Ocean R & D Institute, Ansan 425-170 Korea
E-mail: yiwon@kordi.re.kr
[2]Space Division, Korea Aerospace Research Institute, Taejon 305-333, Korea
[3]Department of Astronomy and Space Sciences, Chungnam National University, Daejon, 363-791

(Received September 7, 1999; Accepted November 4, 1999)

ABSTRACT

A Fourier Transform Spectrometer was used to study upper mesospheric thermodynamics by observing the hydroxyl (OH) emission. Rocket-born and satellite-born photometers place the peak emission near 87 km. The instrument was installed in February 1999 at King Sejong station (62.22 ° S, 301.25 ° E), Antarctica and has been in routine operation since then. An intensive operational effort has resulted in a substantial data set between April and June, 1999. A harmonic analysis was carried out to examine information on the tidal characteristics. The measured amplitudes of the 12-hour oscillation are in the range of 2.4–3.7 K, which are in reasonable agreement with theoretical model outputs. The harmonic analysis also revealed 8-hour oscillation which is not expected from the traditional theoretical studies. In addition, the observed 8-hour oscillations are apparent and sometimes dominate the temperature variation in the upper mesosphere.

1. INTRODUCTION

The lower thermosphere and upper mesosphere is an important region of the atmosphere where processes that dominates in the lower parts of the atmosphere coexist with upper thermospheric process. It is a region where a wide variety of global scale and smaller scale wave forms are linearly superposed on the mean global circulation of the region. It is also a transition region of energy and momentum, and mass transported between the regions below and above. This layer is strongly influenced by semidiurnal tides and gravity waves which propagate upwards from below (Dickinson et al. 1981; Forbes 1985). Smaller scale waves including acoustic and internal gravity waves are known to break near and below this atmospheric layer and turbulent eddies occur here, resulting in large energy deposition (Andrews, Holton, & Leovy 1987). Until recently, this region, between roughly 80–150 km altitude, was the least understood of all atmospheric regions due, in part, to its inherent complexity and due, in part, to the difficulty of carrying out in-situ measurements at this altitude. The complexity and the variability come from a mixture of propagating tides, gravity waves

of multiple origin, planetary waves within this region, and in-situ forcing from solar heating. The lower thermosphere and upper mesosphere region is too high for balloon measurements and too low for in-situ observations by long-lived satellites without on-board propulsion, therefore the data base is exceptionally sparse. As a consequence it has received much less attention than the more readily accessible regions above and below.

The principle dynamical features of the lower thermosphere and upper mesosphere regions are the tidal structures. These oscillations, excited primarily by H_2O insolation absorption in the troposphere and O_3 insolation absorption in the stratosphere and lower mesosphere, propagate upwards and their amplitudes grow exponentially until they reach an altitude where molecular dissipation starts to play a dominant role. Even though the solar forcing is diurnal, the semidiurnal tide (12-hour oscillation) excites efficiently because of its large vertical wavelength and becomes a dominant oscillation in the upper mesosphere and lower thermosphere. On the other hand, the diurnal tide (24-hour oscillation) is trapped and cannot propagate upward except near equatorial latitudes. Because of its deep penetration into the thermosphere, the semidiurnal tide has received more attention than the diurnal tide in scientific studies. Theoretical studies of tides have progressed well since the work of Chapman & Lindzen (1970). A theoretical work of Forbes & Vial (1989) contributed significantly in understanding the solar semidiurnal structure. This theoretical simulation of the solar semidiurnal tide was performed on a global scale for altitude between 80 and 100 km, incorporating a number of physical processes such as molecular and eddy diffusion of heat and momentum, Newtonian cooling, electrodynamic forces, composition variations and interactions with background winds and meridional temperature gradients that were not considered in classical tidal theory.

Ground-based experimental probing of the mesosphere and lower thermosphere has usually been restricted to remote sounding via MF radars or partial reflection systems (Mansoon & Meek 1984), and meteor radars, and light detection and ranging (LIDAR) (Gardner et al. 1989). Recently, there has been a marked improvement in the techniques for measuring the upper mesospheric temperatures by observing a number of OH vibration-rotation bands (Meinel bands) as well as O_2 molecular bands. The hydroxyl (OH) emissions were first identified by Meinel (1950). Since then, many researchers have made ground-based, and rocket-borne observations of individual OH vibrational- rotational bands and identified its peak altitude at 87 $\pm$3 with a half width 5 $\sim$ 8 km (Baker & Stair, 1988). Because rotational relaxation is sufficiently rapid in this region, the distribution of rotational lines within a band is expected to represent the kinetic temperature of the gas. Ground-based measurements of the OH rotational lines therefore provide the atmospheric temperature at this height.

As a part of upper atmospheric research program, the Polar Research Center, Korea Ocean Research & Development Institute(KORDI) has recently equipped a Fourier Transform Spectrometer (FTS) to study thermodynamical characteristics of the Earth's lower thermosphere and upper mesosphere region. The FTS system was tested and installed in February 1999 at King Sejong Station, Antarctica for a continuous monitoring of the Earth's upper atmospheric environment.

In this paper, we describe brief descriptions of the instrument, data acquisition, and analysis procedures and provide some preliminary results.

2. EXPERIMENTS

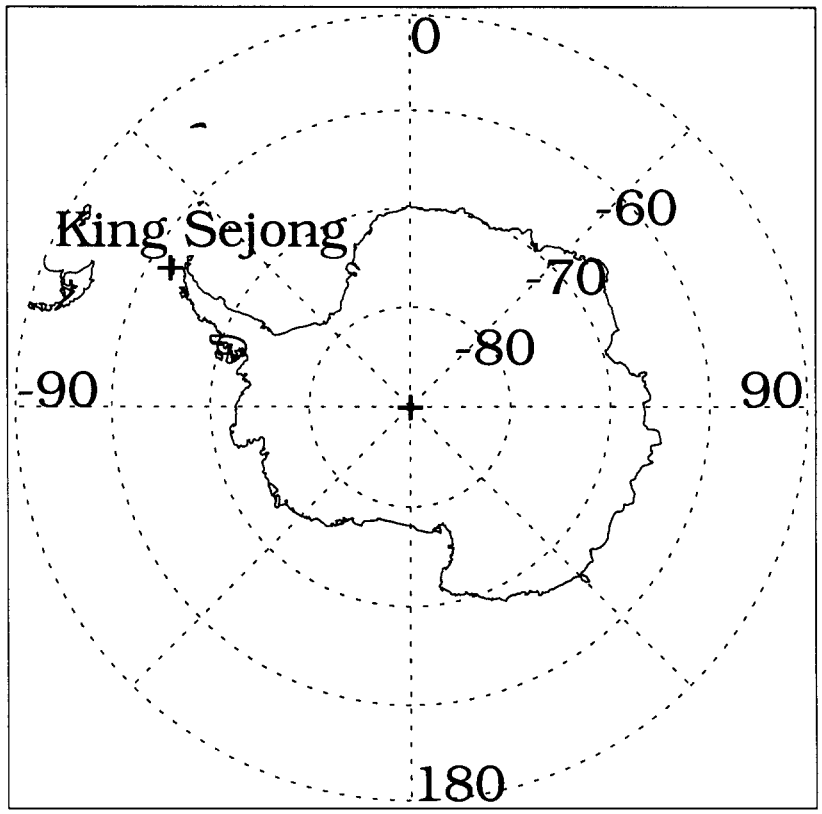

Figure 1. The location of King Sejong station in geographic coordinates.

The polar research center, KORDI has long been involved in performing ground-based optical observations of terrestrial airglow emission at King Sejong station, Antarctica (Figure 1). Airglow observatory in King Sejong station was established in 1989 to monitor the thermospheric OI[630.0 nm] emission utilizing the Fabry-Perot interferometer (FPI) technique (Kim et al. 1989; Chung et al. 1998). As a complement to the existing FPI, the newly equipped FTS system was installed in February 1999 to initiate a program designed to provide long-term measurements of the dynamics in the mesosphere and lower thermosphere over King Sejong station. The newly equipped FTS system is placed inside the small container located in the front-right. A FPI building is also seen in the behind. A heater is placed at the base of the dome to keep it free of condensation at all times. Another heater is placed inside the container to keep the temperature constant. This container will be replaced by a more structured trailer in 2000.

Table 1. The specifications of the Bomem Michelson interferometer.

Spectral range	5000 cm$^-$1 to 10,000 cm$^-$1 (detector response)
Resolution	1, 2, 4, 8, 16 cm$^-$1 (selectable)
Detector	0.5 mm diameter InGaAs detector module (TE-cooled operation)

The FTS system was purchased from Bomem, Inc, Quebec. The instrument is compact and transportable and data acquisition is controlled by a PC type computer. As is written in Table 1, the spectral range of the system is from 5000 cm^{-1} to 10,000 cm^{-1}. The OH Meinel bands within this region include the (4–2) and (3–1) bands of the bright $\Delta\nu = 2$ sequence and the (9–5), (8–5), (7–4), (6–3), (5–2), (4–1) bands of the $\Delta\nu = 3$. As was pointed out by Lowe, Gilber, & Turnbull (1991), P1(1), P1(2) and P1(3) lines in the (3–1) and (4–2) bands are the most intense lines in the hydroxyl spectrum which are not affected to any significant extent by atmospheric absorption. The FTS system employes a thermoelectrically cooled InGaAs detector, which has maximum sensitivity in the wavelength region 1 to 1.65 m. For our study, temperature measurements were determined from three resolved rotational features of the Meinel OH (3-1) band. The (3–1) band was used in this study in preference to the (4–2) band due to the fact that the InGaAs detector response cut-off is very close to the (4–2) band and is rather sensitive to detector temperature.

The system has 5 choices of spectral resolution which is selectable. Increasing the spectral resolution decreases temporal resolution, and the optimum setting of spectral resolution for the accurate calculation of temperatures was set to $8cm^{-1}$. With this resolution, the interferometer records an interferogram every 5 seconds. In order to increase the signal-to-noise ratio, we need to co-add a number of interferograms. However, increasing the number of interferograms reduces the temporal resolution and, therefore, a compromise should be reached between the increase in the S/N ratio and the reduction in the temporal resolution. The number of interferograms co-added for each spectrum was increased until we get resultant temperature error bars in the range of ± 7. For our calculation, interferograms over about a 5-minute period (50 interferograms) were co-added. Then, the composite interferogram was apodized using a cosine-apodization function to reduce the side lobes. The relative spectral response of the detector is determined by calibration with a low brightness source. A near IR source lamp was incorporated for the correction of the spectral response. The low brightness source lamp was supplied from the manufacturer after it was absolutely calibrated by Center for Research in Earth and Space Technology, Ontario, Canada for this purpose. Figure 2 shows a typical spectrum obtained by fourier transforming the apodized interferogram. Note that various vibrational-rotational bands are seen in the spectrum.

Rotational temperature information of hydroxyl emissions is retrieved from the intensity distribution of the rotational lines. The rotational lines to be used in our study are assumed to have intensities which conform to a Boltzmann distribution of OH among the rotational levels of each vibrational state (Sivjee 1992).

For a Boltzmann distribution of multiplet rotational levels, the photon emission intensity of a rotational line at a temperature T_rot is given by the following expression (Mies 1974):

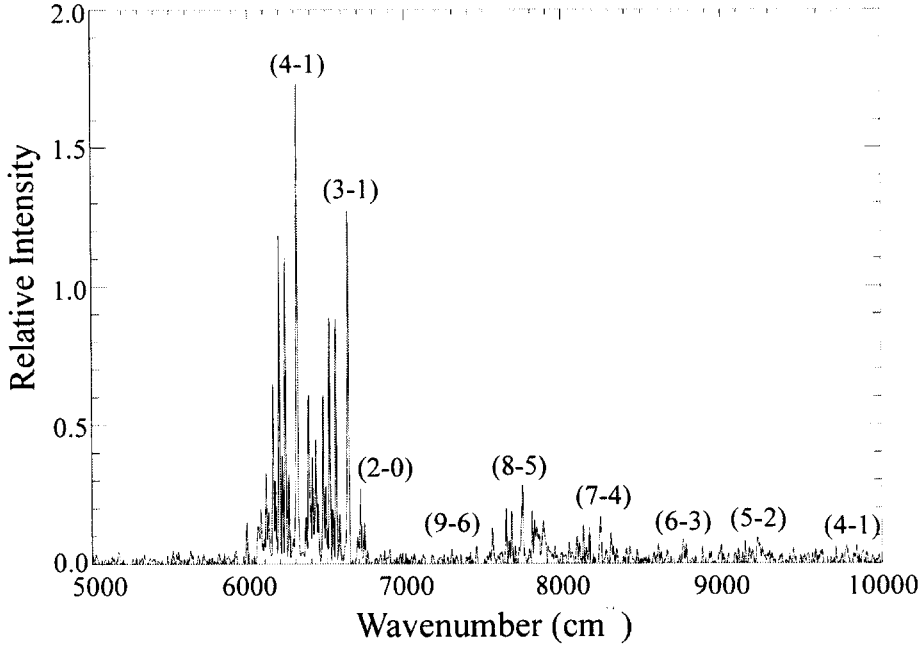

Figure 2. The measured nighttime OH spectrum using our FTS.

$$I_{(J',\nu'\rightarrow J'',\nu'')} = N_{\nu'} A_{(J',\nu'\rightarrow J'',\nu'')} \frac{2(2J'+1)}{Q_{\nu'}(T_{rot})} e^{\frac{-E_{J'}}{kT_{rot}}} \tag{1}$$

where J' is the upper-state total angular momentum, I is the intensity of the vibrational-rotational transition from the state J', ν' to the state J", ν'', k is the Boltzmann constant, $N_{\nu'}$ is the total concentration of molecules in the upper vibrational state, $A(J',\nu' \rightarrow J'',\nu'')$ is the spontaneous Einstein emission coefficient for the vibrational-rotational transition, which is the reciprocal of the expected lifetime of a particular state, and $Q_{\nu'}$ is the partition function or state sum defined as

$$Q_{\nu'}(T) = \sum_{J'} (2J'+1) e^{\frac{-E_{J'}}{kT_{rot}}} \tag{2}$$

Here, $E_{\nu'}(J')$ is the upper state energy. The energy of a state, or its term value, is usually given in units of reciprocal centimeters (cm^{-1}) and is denoted by $F_{\nu'}(J')$, and $E_{\nu'}(J') = F_{\nu'}(J') * 100hc$, where h is Planck's constant and c is the speed of light.

Eq. (1) may be converted to a linear equation in the following form:

$$\ln\left[\frac{I_{(J',\nu'\rightarrow J'',\nu'')}}{2(2J'+1)A_{(J',\nu'\rightarrow J'',\nu'')}}\right] = \ln\left[\frac{N_{\nu'}}{Q_{\nu'}(T_{rot})}\right] - \frac{-F_{\nu'}(J')100hc}{kT_{rot}} \tag{3}$$

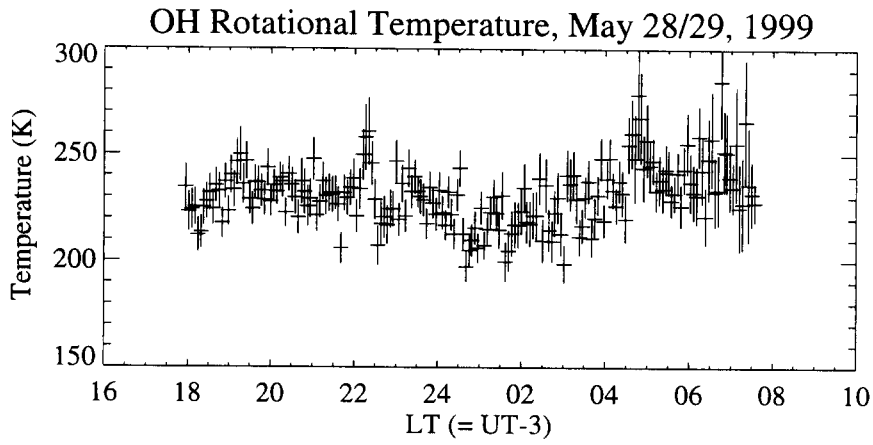

Figure 3. A composite plot of rotational temperature measured on the night of May 28, 1999 with error bars (statistical uncertainties) superimposed.

The slope of a plot of the left-hand side versus $F_{v'}(J')$ yields the rotational temperature. The intercept on the plot was used to determine the intensity of the emission. The detailed information on the analysis of OH rotational temperature and band intensity was described in Won et al. (1999b).

3. RESULTS AND DISCUSSION

The FTS system was installed in February, 1999, and has been in routine operation, making zenith measurements of OH Meinel bands since the middle of March, 1999. An intensive operational effort has resulted in a substantial data set between April and June, 1999 and these data were used for our study. Figure 3 displays a composite plot of the rotational temperatures of OH(3,1) measured on the night of May 28, 1999. Included in the figure are error bars (statistical uncertainties), which are usually less than 10 degrees. The measured temperatures are very high at the start of observation due to the twilight. As in the case for most optical instruments, observations were limited by daylight and the cloud condition.

Usually, the observation was performed only during clear night, but some of measurements were also taken during cloudy condition because of the frequent weather changes during the observation. To avoid these unwanted data, any temperature data with statistical uncertainty over about 10 % of the mean value of the night time temperatures were eliminated. This filtering process seems to be enough to avoid data contaminated by cloud cover and still hold good amount of useful data. The remaining data sets were binned in one hour interval and averaged over a monthly basis to examine the seasonal behavior of upper mesospheric thermodynamics. The summing process over the month would reduce the influence of gravity waves which may be somewhat random in phase (Hecht et

Table 2. OH mean temperature, semidiurnal and terdiurnal amplitudes, and phases at King Sejong station for the three month period. Comparisons are made with the Forbes & Vial (1989) output (in parentheses) at the same latitude for semidiurnal tide.

Month	Mean (K)	12-hour Amplitude	12-hour Phase	8-hour Amplitude	8-hour Phase
April	210.6 ± 0.4	3.6 ± 0.9 (1.1)	23.7 ± 0.6 (17.2)	6.4 ± 0.9	20.0 ± 0.1
May	225.5 ± 0.2	2.4 ± 0.3 (0.8)	18.1 ± 0.4 (17.4)	1.4 ± 0.3	22.3 ± 0.3
June	218.5 ± 0.3	3.7 ± 0.5 (0.7)	18.7 ± 0.3 (17.6)	4.2 ± 0.5	24.3 ± 0.2

al., 1995) and would result in the tidal information. To retrieve information on tidal oscillation, the resultant data set was fitted in a least square sense with a sinusoidally varying function consisting of a mean term and 12, and 8-hour oscillations as follows:

$$a_0 + a_1 \cos\left(\frac{2\pi t}{12}\right) + b_1 \sin\left(\frac{2\pi t}{12}\right) + a_2 \cos\left(\frac{2\pi t}{8}\right) + b_2 \sin\left(\frac{2\pi t}{8}\right) \quad (4)$$

The amplitude for each wave is calculated by taking $(a_i + b_i)^2$ and the phase is give by the arctangent of the ratio, arctan (b_i/a_i). In fact, we have tried the fitting including diurnal oscillation at first, but found that the magnitudes of the diurnal amplitude were unrealistically high. These spurious diurnal oscillations may be resulted from the fact that the data do not cover the entire 24 hour period (Crary & Forbes 1979), and therefore were omitted in the subsequent procedure.

Figure 4 displays the average temperatures for three month in 1999, with fitting results superimposed (dotted lines). The error bars indicate the weighted uncertainty of the mean value for each hour-bin interval and are usually less than 1 K. The fitting lines represent the measured temperature variation reasonably well, implying that the semidiurnal and terdiurnal components are important oscillations in the upper mesosphere over King Sejong station. Amplitudes, phases (time of maximum) and mean values determined from the fitting results are shown in Table 2, together with model output for semidiurnal tide at the similar latitude (Forbes & Vial, 1989). The Forbes & Vial model incorporates new specifications of zonally averaged wind, temperature and dissipation coefficients and provides monthly simulations of the solar semidiurnal tide in the 80–100 km height regime. Uncertainties in the least squares values were typically less than ± 1 K for the amplitudes and ± 0.5 hour for the phases. The mean temperatures are in the range of ~ 210–225 K, which are in good agreement with other measurements taken at high-latitudes (Walterscheid et al., 1986, Hernandez, Smith, & Conner 1992).

Model calculation of semidiurnal tide at 87 km height predicts the amplitude near 1.0 K in the similar latitude, which is slightly less than those observed at King Sejong station. This is not unusual, though, because most optical and radar observations, regardless of their locations, revealed higher semidiurnal amplitudes than the model output (Walterscheid et al. 1986; Avery et al 1989; Vincent, Tsuda & Kato 1989; Niciejewski & Killeen 1995). In particular, Walterscheid et al. (1986) reported a large-amplitude 12-hour temperature variation (~ 13 K) in their measurements, which is at least an

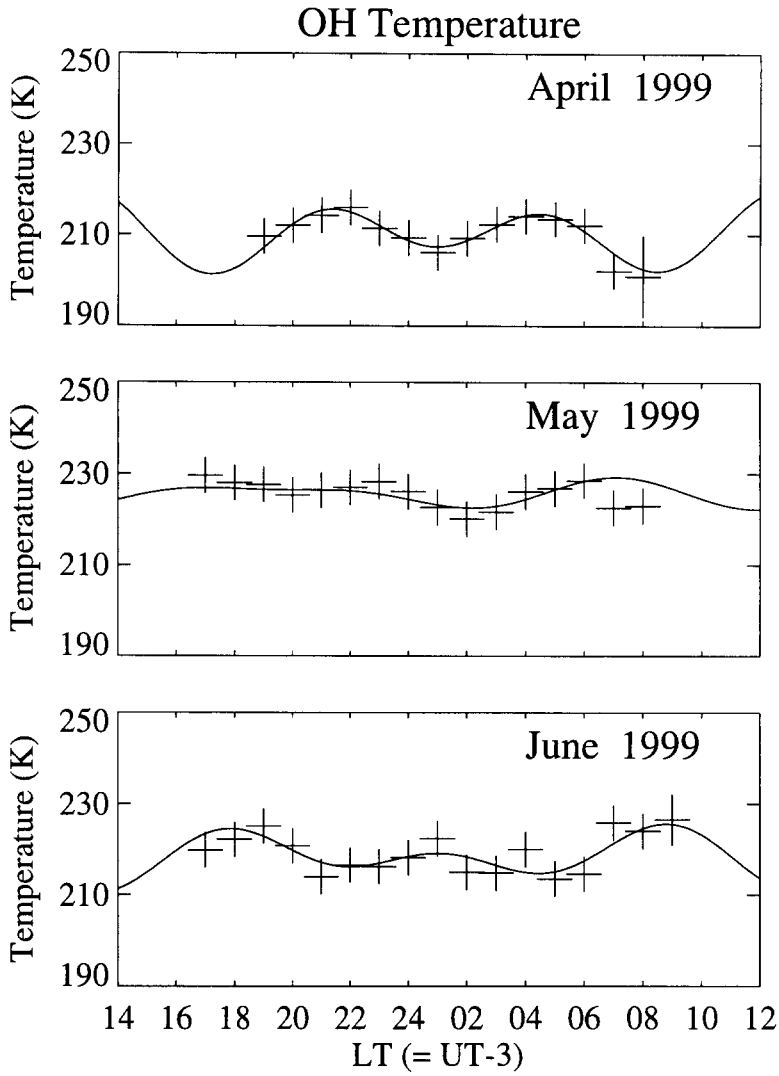

Figure 4. Upper mesospheric temperatures at King Sejong station for three months in 1999. The data have been averaged in 1-hour bin, and a weighted mean has been calculated for each bin. Error bars represent the uncertainty of the mean. Superimposed on the data are the semidiurnal and terdiurnal fits(dotted curve) to the data.

order of magnitude larger than the model prediction and is cannot be described as a normal tide. This, what they called 'pseudotide', was interpreted as a result of gravity wave-mean flow interactions modulated by the solar-driven tide. The plausibility of the interaction between the gravity wave and the mean flows is known to be enhanced by the relatively large semidiurnal tidal-wind speeds as semidiurnal tidal wind velocities are not proportionately as small as temperature oscillations at high latitudes because the latitudinal structure functions for the wind components decay toward the poles much more slowly than do the temperature functions (Walterscheid et al 1986). It would require, however, simultaneous measurements of upper mesospheric neutral winds to clear above process.

The related semidiurnal phases from the measured values are differed less than two hours compared with the model output except for the April result. The observed discrepancy, especially for the April case could be explained by the rapid change of mesospheric structure during equinox season. Nevertheless, the stability of the amplitudes and the reasonable agreement with model calculation (both in amplitude and phase) support the observed 12-hour waves being of tidal origin.

Perhaps the most interesting result to note from our measurements would be the existence of 8-hour oscillation (or waves with periods near 8 hour). As is seen in Figure 4 (and Table 2), the 8-hour oscillation sometimes dominates the temperature variation. The magnitude of terdiurnal oscillation is about twice as large as that of semidiurnal oscillation in April, while even for May and June, these are still comparable to semidiurnal amplitudes. Unlike the semidiurnal oscillation, less attention has been paid to 8-hour oscillation, simply because there is not a strong source to make it become a major oscillation. However, there are several reports that support the existence of the terdiurnal oscillation in the upper mesosphere and lower thermosphere region. One possible source of the 8-hour oscillation, as was discussed by Glass & Fellous (1975), could be the nonlinear interaction between the diurnal and semidiurnal tides. Numerical simulation by Teitelbaum et al. (1989) revealed this nonlinearly generated 8-hour tide was comparable to that of solar-driven 8-hour tide. Won et al. (1999a) also noticed the 8-hour oscillations in their lower thermospheric wind measurements in Greenland, but the observed 8-hour oscillations in their individual data series were regarded as transient because they disappeared in the seasonal average. The 8-hour oscillations in our measurements, however, are resulted from monthly average, hence cannot be ascribed to transient ones, though their amplitudes and phases show some fluctuations. We also admit the possibility that the feature that we interpret as an 8-hour tide may be a gravitational normal mode. As was studied from model simulations by Meyer & Forbes (1997), there are various natural oscillations between 7 and 10 hours in the lower thermosphere and upper mesosphere region, which respond dominantly to the forces over a range of periods. Because of the measurement errors and the short span of data, it is hard to distinguish the observed 8-hour oscillation from the nearby gravitational normal modes.

4. CONCLUSIONS

Fourier Transform spectrometer observations of the mesospheric hydoroxyl emission have been made at King Sejong station since February, 1999. A harmonic analysis to data set between April and June, 1999 was performed to examine major low-frequency oscillations. The measured amplitudes and phases of the 12-hour oscillation are in reasonable agreement with theoretical model output. In addition to the semidiurnal tide, the 8-hour oscillations are also apparent and sometime dominate the

temperature variation, unlike the expectation from the traditional tidal theory.

ACKNOWLEDGMENTSThis work was supported by the grants from Korea Ocean R & D Institute, PP99001-05 and E400001-01.

REFERENCES

Andrews, D. G., J. R. Holton, & C. B. Leovy 1987. Middle Atmosphere Dynamics (San Diego : Academic Press), 489

Avery, S. K., R. A. Vincent, A. Philips, A. H. Manson, & G. J. Fraser 1989, J. Atmos. Sol. Terr. Phys., 51, 595

Baker, D. J. & A. T. Stair, Jr. 1988, Physica Scripta, 37, 611

Chapman, S., & R. S. Lindzen 1970, in Atmospheric Tides (Dordrecht : Reidel), 200

Chung, J. K, Y.-I. Won, B. Y. Lee, & J. Kim 1998, JA&SS, 15, 139

Crary, D. J, & J. M. Forbes 1979, GRL, 10, 580

Dickinson, R. E., E. C. Ridley, & R. G. Roble 1981, JGR, 86, 1499

Forbes, J. M. 1985, J. Atmos. Sol. Terr. Phys., 6, 1049

Forbes, J. M., & F. Vial 1989, J. Atmos. Sol. Terr. Phys., 51, 649

Glass, M, & J. L. Fellous 1975, in Space Research XV (Berlin : Akademie), 191

Gardner, C. D., D. C. Senft, T. J. Beatty, R. E. Bills, & C. A. Hostetler 1989, in WITS Handbook, vol. 2, edited by C. H. Liu (Univ. of Illi., Urbana), 148

Hecht, J. H, S. K. Ramsay Howat, R. L. Walterscheid, & J. R. Isler 1995, JGR, 22, 2817

Hernandez, G., R. W. Smith, & J. F. Conner 1992, GRL, 19, 53

Kim, J. S., Y. Kim, G. S. N. Murty, & J. W. Kim 1990, JKPS, 23, 253

Lowe, R. P., K. L. Gilbert, & D. N. Turnbull 1991, PSS, 39, 1263

Mansoon, A. H. & C. E. Meek 1984, PSS, 32, 1087

Meyer, C. K., & J. M. Forbes 1997, J. Atmos. Sol. Terr. Phys., 59, 2185

Meinel, A. B. 1950, ApJ., 111, 555

Mies, F. H. 1974, J. Mol. Spectros., 53, 150

Niciejewski, R. J., & T. L. Killeen 1995, JGR, 100, 25855

Sivjee, G. G. 1992, PSS, 40, 235

Teitelbaum, H. F., F. Vial, A. H. Manson, R. Giraldez, & M. Massebeuf 1989, J. Atmos. Sol. Terr. Phys., 51, 627

Vincent, R.A., T. Tsuda, & S. Kato 1989, J. Atmos. Sol. Terr. Phys., 51, 609

Walterscheid, R. L., G. G. Sivjee, G. Schubert, & R. M. Hamwey 1986, Nature, 324, 347

Won, Y.-I., R. J. Niciejewski, T. L. Killeen, R. M. Johnson, & B. Y. Lee 1999a, JGR, 104, 25

Won, Y.-I., J.-K. Chung, B. Y. Lee, J. Kim, & J. B. Kim 1999b, JKPS, 34, 344